11th World Congress on Computational Mechanics (WCCM XI)
5th European Conference on Computational Mechanics (ECCM V)
6th European Conference on Computational Fluid Dynamics (ECFD VI)
E. Oñate, J. Oliver and A. Huerta (Eds)

AN INVESTIGATION OF COOLING CHARACTERISTICS IN AIR-MIST COOLING BY EULERIAN-LAGRANGIAN METHOD WITH V2F MODEL

TSUYOSHI YAMAMOTO*, KAKERU YOSHINO* AND TAKUYA KUWAHARA*

* Department of Chemical Engineering
Kyushu University
744 Motooka, Nishi-ku, Fukuoka, 819-0395, Japan
e-mail: yamamoto@chem-eng.kyushu-u.ac.jp, www.kyushu-u.ac.jp

Key Words: *Mist cooling, Fine Mist, High Heat Flux, V2F Model.*

Abstract. Heat transfer techniques involving phase a change process are likely to play an important role in industrial devices that require the ability to remove high heat quickly. Air-mist cooling, which has a low energy cost and a low environmental load, is a technology to cool high temperature surface using the latent heat associated with the vaporization of atomized droplets. In the present work, air-mist cooling as a high heat removal technology has been applied to the cooling of heated wall. A three dimensional numerical simulation, which is based on two fluid model using Eulerian-Lagrangian method with V2F model, has been developed in order to investigate the cooling characteristics of heated wall. It is found that the wall temperature rapidly decreases due to the effect of latent heat in the early stage of air-mist cooling, because there has the high rate of evaporation of fine mist particles on the wall.

1 INTRODUCTION

Mist cooling [1,2] is a very efficient technique for dissipating high heat fluxed with low coolant mass fluxes at low wall superheats. It is used in a wide range of applications from metal quenching over cooling of high power electronics to medical treatments. The heat transfer capability of mist cooling has greatly improved, and it has been reported that heat fluxes of mist cooling using water as coolant increased up to 1000 W/cm^2 [3]. The coolant forms a cohesive or ruptured thin liquid film, which evaporates on the hot surface, depending on the mist parameters and surface properties. The transferred heat flux increases at a given surface temperature with decreasing film thickness [3]. From that result, the effects of mist cooling parameters (mean droplet size, droplet flux and droplet velocity) on critical heat flux were studied [4]. The experimental study was conducted to investigate the effect of surface structures and coolant mass flux on the heat transfer in the low surface temperature regime [5]. Recently, since water droplets of mist become smaller and vaporize more easily with the advance of atomization technologies, the outdoor cooling technology, which is called dry mist or dry fog, has been put into practical use [6].

Many industrial devices require the abilities to remove high heat quickly with the development of industry in the region of high speed electrical components [7] or high power

leasers [8] and so on. These requests will not be met by the limited capacity of conventional cooling technologies such as forced convection. In order to apply fine mist cooling to industrial devices and develop to a higher level, it is necessary to understand the heat and mass transfer of fine mist cooling in detail. However, it is difficult to understand the transport phenomena of fine mist cooling only using experiments, because fine mist cooling is a complex two phase flow with droplet evaporation, latent heat and convection heat. A numerical simulation is a powerful tool for better understanding of the transport phenomena of fine mist cooling. There have been little studies that investigated the heat and mass transfer of fine mist cooling in detail using the numerical simulation.

In the present work, we have paid the attention to evaporative latent heat of fine mist, which has very small particles of several ten micrometers in diameter and easily evaporates. The objective of present work is to apply the air-mist cooling as a high heat removal technology to the cooling of high temperature industrial devices. The comprehensive simulation model, which is based on two fluid model using Eulerian-Lagrangian method with V2F model, has been constructed in order to analyze the air-mist cooling intended for high temperature iron laminated wall. A three dimensional numerical simulation has been carried out to investigate the behavior of fine mist particles, flow of gas phase and temperature distribution of wall.

2 NUMERICAL SIMULATION

Figure 1 shows a schematic diagram of air-mist cooling system. This system consists of air-mist nozzle, iron wall and heater. The air-mist nozzle is a two phase fluid nozzle to spray air-mist including water droplets and air. The iron wall is 300 mm in height, 300 mm in width and 17 mm in thickness. The air-mist nozzle is set in position of 200 mm from the wall and cools the wall heated from back side. Table 1 shows a numerical simulation conditions. As shown in Table 1, the environmental temperature is 298 K and the environmental humidity is 60 %. The wall material is a iron plate. It is heated up and the initial temperature of wall is set to 373 K. Air is fed 36 nL/min under pressure 0.3 MPa into the air-mist nozzle by a compressor and water is added 2.4 L/hr to the air-mist nozzle by pressure controlled water tank at 0.1 MPa. The air-mist nozzle sprays the fine mist, which is composed of atomized water droplets and air, into the heated wall. The starting time is the initiation of air-mist cooling and the output of heater keeps constant at 360 W. Additionally, as compared with the numerical simulation, the experiment has been performed on same conditions as the numerical simulation, which is shown in Fig. 1 and Table 1. In experiment, the iron wall is laminated by four plates, which are 1 mm, 3 mm, 3 mm and 10 mm in thickness. The temperatures of wall are measured at 12 positions, which are 1 mm, 4 mm and 7 mm in thickness direction and 0 mm, 40 mm, 80 mm and 120 mm in radial direction, by K type bare thermocouples.

The numerical simulation has been performed in three dimensional rectangular coordinate. Air-mist cooling is modeled as a two-phase flow system of a gaseous phase and particle phase. The gaseous phase is treated by an Eulerian method and the particle phase is calculated by a Lagrangian particle tracking method. The gaseous phase and particle phase are coupled by the PSI-CELL (Particle-Source-In Cell) Model [9]. The internal temperature of wall is simulated by a heat conduction equation with consideration for the contact thermal resistance.

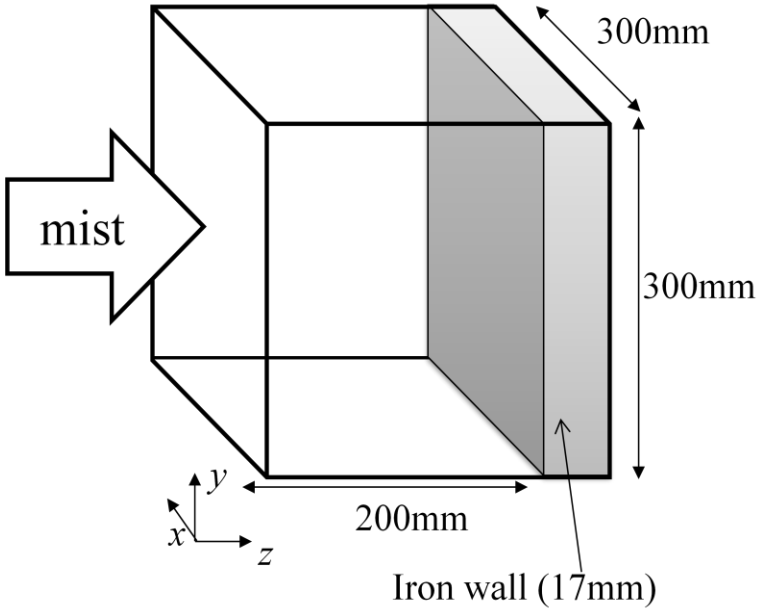

Figure 1: Schematic diagram of air-mist cooling system.

Table 1: Numerical simulation conditions

Environmental temperature	[K]	298
Environmental humidity	[%]	60
Air feed rate	[nL/min]	36
Supply pressure of air	[MPa]	0.3
Water feed rate	[L/hr]	2.4
Pressure of water tank	[MPa]	0.1
Heater input	[W]	360
Initial temperature of wall	[K]	370

2.1 Gas phase

The unsteady state gas flow is described by continuity equation and conservation equation of mass, momentum, chemical species and enthalpy. The effective viscosity due to turbulent is modeled by means of v^2-f model [10].The general form of the governing equation in three-dimensional rectangular coordinate is:

$$\frac{\partial}{\partial t}(\rho\phi)+\frac{\partial}{\partial x}(\rho u\phi)+\frac{\partial}{\partial y}(\rho v\phi)+\frac{\partial}{\partial z}(\rho w\phi)=\frac{\partial}{\partial x}\left(\Gamma_\phi\frac{\partial\phi}{\partial x}\right)+\frac{\partial}{\partial y}\left(\Gamma_\phi\frac{\partial\phi}{\partial y}\right)+\frac{\partial}{\partial z}\left(\Gamma_\phi\frac{\partial\phi}{\partial z}\right)+S_\phi+ \quad (1)$$

ϕ = 1(mass), u, v, w, k, ε, $\bar{v}^2$, h, m_i

where the equation for ϕ = 1 is mass conservation equation, whereas u, v and w equations are the momentum equations for x, y and z direction, respectively. k, ε and $\bar{v}^2$ are kinetic energy of turbulence, its dissipation rate and velocity scale in v^2-f model. h and m_i are stagnation enthalpy and mass fraction for chemical species of i (i = H_2O, O_2, N_2). The dependent variables ϕ, the effective exchange coefficients Γ_ϕ in the diffusive term and the source term S_ϕ

are shown in Table 2. $S_{p\phi}$ represents the mass, momentum and enthalpy exchanges between gas flow and particles.

Table 2: Dependent variables, source terms and turbulent diffusion coefficients for gas governing equations.

	ϕ	Γ_ϕ	S_ϕ
Mass	1	0	0
Velocity component	u	μ_{eff}	$\frac{\partial}{\partial x}\left(\mu_{\text{eff}}\frac{\partial u}{\partial x}\right)+\frac{\partial}{\partial y}\left(\mu_{\text{eff}}\frac{\partial v}{\partial x}\right)+\frac{\partial}{\partial z}\left(\mu_{\text{eff}}\frac{\partial w}{\partial x}\right)-\frac{\partial P}{\partial x}$
	v	μ_{eff}	$\frac{\partial}{\partial x}\left(\mu_{\text{eff}}\frac{\partial u}{\partial y}\right)+\frac{\partial}{\partial y}\left(\mu_{\text{eff}}\frac{\partial v}{\partial y}\right)+\frac{\partial}{\partial z}\left(\mu_{\text{eff}}\frac{\partial w}{\partial y}\right)-\frac{\partial P}{\partial y}$
	w	μ_{eff}	$\frac{\partial}{\partial x}\left(\mu_{\text{eff}}\frac{\partial u}{\partial z}\right)+\frac{\partial}{\partial y}\left(\mu_{\text{eff}}\frac{\partial v}{\partial z}\right)+\frac{\partial}{\partial z}\left(\mu_{\text{eff}}\frac{\partial w}{\partial z}\right)-\frac{\partial P}{\partial z}$
Kinetic Energy	k	$\mu_{\text{eff}}/\sigma_k$	$G_k-\rho\varepsilon$
Dissipation rate	ε	$\mu_{\text{eff}}/\sigma_\varepsilon$	$\frac{1}{T}\left(C_{\varepsilon 1}G_k-C_{\varepsilon 2}\rho\varepsilon\right)$
Velocity scale	$\bar{v}^2$	$\mu_{\text{eff}}/\sigma_k$	$kf-\frac{\bar{v}^2}{k}\varepsilon$
Mass fraction	m_i	$\mu_{\text{eff}}/\sigma_m$	$w_{ij}R_i$
Enthalpy	h	$\mu_{\text{eff}}/\sigma_h$	0

$$f-L^2\left\{\frac{\partial}{\partial x}\left(\frac{\partial f}{\partial x}\right)+\frac{\partial}{\partial y}\left(\frac{\partial f}{\partial y}\right)+\frac{\partial}{\partial z}\left(\frac{\partial f}{\partial z}\right)\right\}=(C_1-1)\frac{(2/3-\bar{v}^2/k)}{T}+C_2\frac{P}{k}$$

$$T'=\max\left(\frac{k}{\varepsilon},6\left(\frac{v}{\varepsilon}\right)^{1/2}\right),\quad T=\min\left(T',\frac{\alpha}{\sqrt{3}}\frac{k}{\bar{v}^2C_\mu\sqrt{2S^2}}\right)$$

$$L=C_{\text{L}}\max\left(\frac{k^{3/2}}{\varepsilon},C_\eta\left(\frac{v^3}{\varepsilon}\right)^{1/4}\right)$$

$$\mu_{\text{t}}=C_\mu\rho\bar{v}^2T$$

$$\mu_{\text{eff}}=\mu+\mu_{\text{t}}$$

$$G_k=\mu_{\text{eff}}\left[2\left\{\left(\frac{\partial u}{\partial x}\right)^2+\left(\frac{\partial v}{\partial y}\right)^2+\left(\frac{\partial w}{\partial z}\right)^2\right\}+\left(\frac{\partial u}{\partial y}+\frac{\partial v}{\partial x}\right)^2+\left(\frac{\partial w}{\partial y}+\frac{\partial v}{\partial z}\right)^2+\left(\frac{\partial u}{\partial z}+\frac{\partial w}{\partial x}\right)^2\right]$$

$$C_{\varepsilon 2}=1.44\left(1+0.045\sqrt{\frac{k}{\bar{v}^2}}\right)$$

C_μ	$C_{\varepsilon 2}$	C_1	C_2	C_{L}	C_η	σ_k	σ_ε	σ_m	σ_h
0.19	1.92	1.4	0.3	0.3	70.0	1.0	1.3	0.9	0.9

2.2 Forced convection heat transfer by impinging jet

The heat flux of forced convection is expressed as equation (2) based on wall function [11].

$$q_{\mathrm{c}} = \frac{(T_{\mathrm{wall}} - T)\rho C_{\mathrm{P}} {C_{\mu}}^{1/4} k^{1/2}}{Pr_{\mathrm{t}}\left[\frac{1}{\kappa}\ln(Ey^{+}) + P\right]} \tag{2}$$

where P is represented as [12]:

$$P = 9.24\left[\left(\frac{Pr}{Pr_{\mathrm{t}}}\right)^{3/4} - 1\right]\left[1 + 0.28\exp\left(-0.007\frac{Pr}{Pr_{\mathrm{t}}}\right)\right] \tag{3}$$

2.3 Heat conduction in the wall

The equation of heat conduction in the wall is expressed as:

$$\rho C_{\mathrm{P}}\frac{\partial T}{\partial t} = \frac{\partial}{\partial \mathrm{x}}\left(\lambda\frac{\partial T}{\partial x}\right) + \frac{\partial}{\partial \mathrm{y}}\left(\lambda\frac{\partial T}{\partial y}\right) + \frac{\partial}{\partial \mathrm{z}}\left(\lambda\frac{\partial T}{\partial z}\right) + S \tag{4}$$

The contact thermal resistance is considered in the wall, because the wall is laminated by four plates in the experiment. It is assumed that the thicknesses of air layer between the wall are constant. The contact thermal resistance is represented as:

$$R_{\mathrm{c}} = \left(\frac{d - d_{air}}{\lambda} + \frac{d_{air}}{\lambda_{air}}\right)\Big/\mathrm{A} \tag{5}$$

where d is grid thickness and d_{air} is the thickness of air layer.

2.4 Dispersed particle tracking

The particle momentum equation and energy conservation equation are:

$$\frac{du_{pi}}{dt} = \frac{3}{4}\frac{\mu}{\rho_{\mathrm{p}} d_{\mathrm{p}}^2} C_D Re_{\mathrm{p}}(u_i - u_{\mathrm{p}i}) + g_i \tag{6}$$

$$C_{\mathrm{p}} m_{\mathrm{p}}\frac{dT_{\mathrm{p}}}{dt} = \pi d_{\mathrm{p}}^2 h_c(T_{\mathrm{g}} - T_{\mathrm{p}}) + L_h\frac{dm_{\mathrm{p}}}{dt} + \sigma_{st} A\frac{T_w^4 - T_p^4}{1/\varepsilon_w + 1/\varepsilon_p} + \lambda A\frac{(T_{\mathrm{w}} - T_{\mathrm{p}})}{dt} \tag{7}$$

where C_D denotes the drag coefficient, which is a function of the particle Reynolds number Re_{p}. μ, ρ_{p} and d_{p} are the gas viscosity, particle density and particle diameter, respectively. σ_{st} and ε are Stefan-Boltzmann constant and emissivity. The turbulent dispersion of particle is described by the gas velocity fluctuation vector which obeys a Gaussian probability density function having a standard deviation $(2k/\varepsilon)^{0.5}$. Particle-particle interaction is negligible in this work. If the particle is collided with the wall, the fluid calculation of particle is suspended and it considers that the particle is adhered to the wall. In the equation (7), the first term, second term and third term on the right side represent the convection heat transfer, latent heat of water and radiation heat transfer, respectively. The fourth term on the right side represents the conduction heat transfer, and this term is considered only after the particle is adhered to the wall. Where h_c is the coefficient of convective heat transfer and is expressed as:

$$h_c = \frac{\lambda}{d_\mathrm{p}}\left(2 + 0.6Re^{1/2}Pr^{1/3}\right) \tag{8}$$

The rate of droplet mass [13], which is evaporated during the time interval, is represented as:

$$\frac{dm_\mathrm{p}}{dt} = \pi d_\mathrm{P}^2 \frac{h_\mathrm{m}}{R}\left(\frac{P_{sat}}{T_\mathrm{P}} - \frac{P}{T}C\right) \tag{9}$$

where P_{st} and C are the saturated vapor pressure at the droplet temperature and water vapor concentration, respectively. hm is mass transfer coefficient and is calculated from the following equation.

$$Sh = \frac{h_\mathrm{m} d_\mathrm{P}}{D} = 2 + 0.6Re^{0.5}Sc^{0.33} \tag{10}$$

where *Sh* and *Sc* are Sherwood number and Schmidt number, respectively. *D* is diffusion coefficient.

2.5 Droplet size distribution

Figure 2 shows the size distribution of fine mist droplets sprayed from two-phase fluid air-mist nozzle. In this simulation, the size distribution of the droplets is expressed as a log normal distribution from 3 to 22 μm, because it has a correlate with experimental results as shown in Fig. 2. The distribution is divided into 20 ranges and 200 computational droplets are assigned in each range. The injection angle of droplet is chosen randomly from a Gaussian distribution to represent the air-mist nozzle spray pattern.

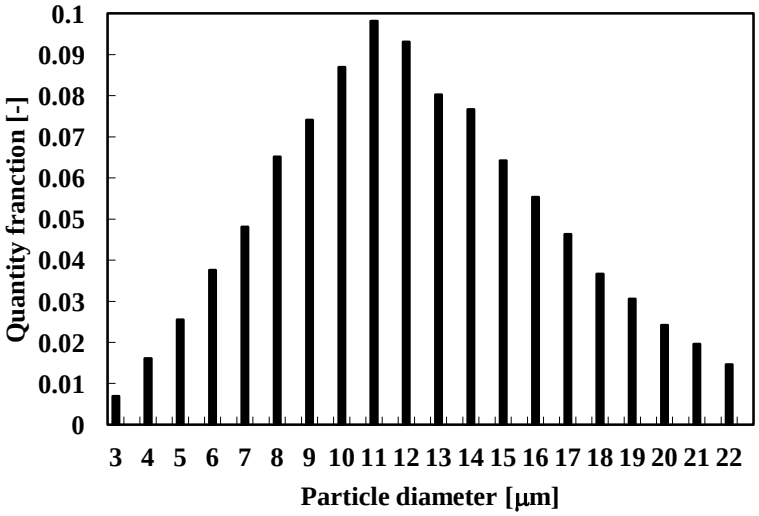

Figure 2: Size distribution of fine mist droplets sprayed from two-phase fluid air-mist nozzle.

2.6 Numerical solution

The conservation equation (1) is discretized using a finite volume code with a staggered grid arrangement and discretized coefficients are calculated by Power-Law scheme [14]. The partial differential equation shown in Eq. (1) is solved by employing the SIMPLE (Semi-Implicit Method for Pressure Linked Equations) algorithm [15]. The velocity, pressure

increment and scalar fields are solved using the Bi-Conjugate Gradient Stabilized (Bi-CGSTAB) [16]. Fourth-order Runge-Kutta-Gill method is used to solve the conversation equations (6) - (10) for a particle. And mass, velocity components, position and temperature of particle are calculated at each time. The environmental temperature and the environmental humidity are used at boundary except for the wall and Neumann condition is applied in the outflow boundary.

3 RESULTS AND DISCUSSION

Figure 3 shows the time changes of surface temperature at the center of wall compared between calculation results and experimental results. Figure 4 shows the surface temperature distribution of the wall after steady state compared between simulation results and experimental results. Model predictions reproduce a rapid drop well for the surface temperature of wall at the beginning of air-mist cooling. The surface temperature of wall becomes steady state condition after about 5000 s and the calculated surface temperature of wall is in reasonably good agreement with the experimental result.

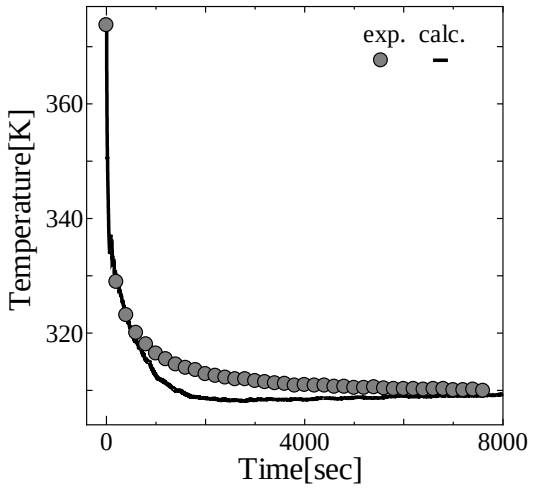

Figure 3: The time changes of surface temperature at the center of wall compared between calculation results and experimental results.

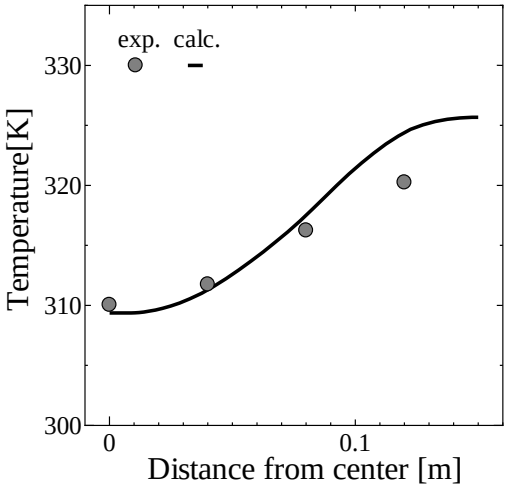

Figure 4: The surface temperature distribution of the wall after steady state compared between calculation results and experimental results.

Figure 5 shows the predicted temperature distribution and velocity vector of gas phase at x-z cross section of central axis and x-y cross section near the laminated wall after steady state condition. Figure 6 shows the simulated water particle trajectories. After the air jetted from nozzle impinges on the wall with a little spread, it uniformly spreads out from the center of wall and flows outside the analytical region. The gas temperature near the wall increases with distance from the center of wall, because the gas is heated by heat exchange with the wall. Water droplets move near the wall with gas phase under the influence of drag force and turbulence fluctuation. And then there are observed four cases that they completely evaporate in gas phase, they directly collide with the wall by inertial force, they impinge on the wall with spreading along the flow of gas phase, and they flow outside the analytical region. Water droplets impinge on the stagnation region with high frequency and collision frequency

decreases with distance from the stagnation region. As a consequence, the wall has the lowest surface temperature at stagnation point due to the latent heat and the surface temperature of wall increases with distance from the stagnation point. The surface temperatures at 0 mm, 40 mm, 80 mm and 120 mm from the center of wall are 309 K, 311 K, 317 K and 324 K, respectively.

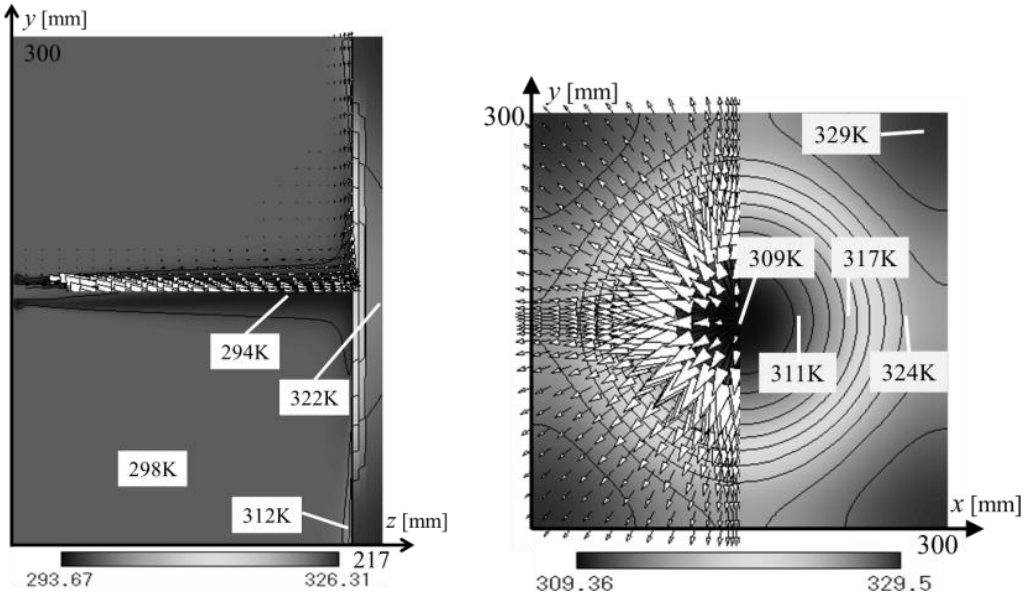

(a) y-z cross section (b) x-y cross section

Figure 5: Predicted temperature distribution and velocity vector of gas phase after steady state condition

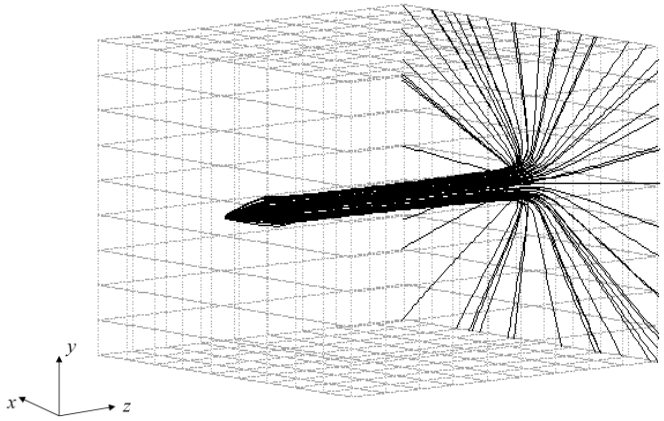

Figure 6: Simulated trajectories of fine mist particles.

The behavior of fine mist particles in the numerical simulation are classified four categories, which are evaporation in gas phase, flowing out of analytical region, evaporation on the wall after impinging the wall and staying on the wall after impinging the wall. Figure 7 shows the calculated time changes of the rate of evaporation in gas phase, impinging the wall and flowing out of analytical domain for fine mist particles. Figure 8 shows the simulated

time changes of the rate of evaporation on the wall and staying on the wall after impingement. Model prediction indicates that 8.7 wt% of fine mist particles evaporate in gas phase, 85.8 wt% of fine mist particles impinge on the wall and 5.5 wt% flow out of analytical domain immediately after the beginning of spray. After steady state 0.7 wt% of fine mist particles evaporate in gas phase, 89.3 wt% of fine mist particles impinge on the wall and 10.0 wt% flow out of analytical domain. The fine mist particles hardly evaporate in gas phase after steady state, because there is little difference in temperature between fine mist particles and gas phase, and the humidity level is high. 3.5 wt% out of those particles, which do not evaporate in gas phase, impinge on the wall and 4.5 wt% flow out of analytical domain. After fine mist particles impinge on the wall, 66.7 wt% of fine mist particles evaporate on the wall and 19.1 wt% of fine mist particles stay on the wall immediately after the beginning of spray. After steady state 7.1 wt% of fine mist particles evaporate on the wall and 82.2 wt% of fine mist particles stay on the wall. Since the initial conditions are that the environmental humidity is 60 % and the laminated wall temperature is 373 K, water droplets easily receive a heat from the wall and easily evaporate on the wall at the beginning of air-mist cooling. As a results, there has the high rate of evaporation of water droplets on the wall in the early stage of air-mist cooling, the wall temperature rapidly decreases due to the effect of latent heat. The relative humidity of gas phase increases and the surface temperature of wall decreases with an increasing amount of water droplets evaporation. The water droplets on the wall have the property that the evaporation proportion decreases and the staying proportion increases with an increasing time.

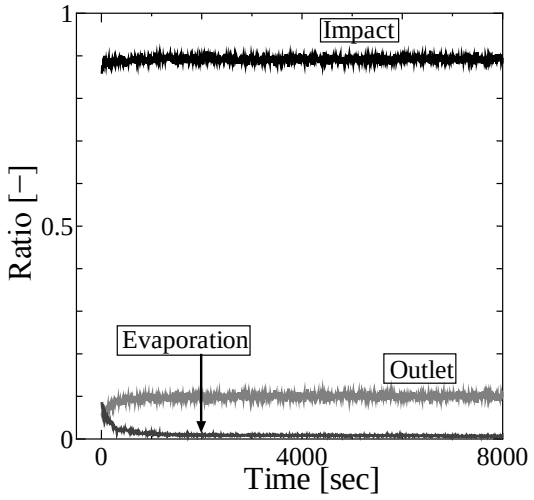

Figure 7: The time changes of the rate of evaporation in gas phase, impinging the wall and flowing out of analytical domain for fine mist particles.

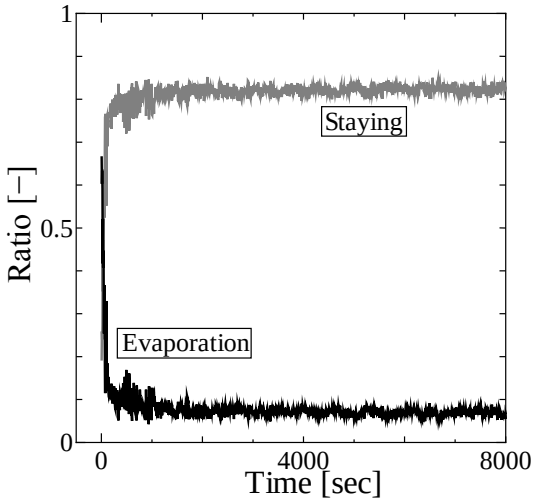

Figure 8: The time changes of the rate of evaporation on the wall and staying on the wall after impingement.

4 CONCLUSIONS

The comprehensive simulation model based on two fluid model using Eulerian-Lagrangian method with V2F model has been developed in order to simulate air-mist cooling intended for the iron wall. Air-mist cooling characteristics such as the behavior of fine mist particles, flow

of gas phase and temperature distribution of wall has been investigated. Model prediction are in reasonably good agreement with the experimental data. Simulation results indicate that 8.7 wt% of fine mist particles evaporate in gas phase, 85.8 wt% of fine mist particles impinge on the wall and 5.5 wt% flow out of analytical domain immediately after the beginning of spray. After impingement, 66.7 wt% of fine mist particles evaporate on the wall and 19.1 wt% of fine mist particles stay on the wall at the beginning of air-mist cooling. As a consequence, there has the high rate of evaporation of water droplets on the wall in the early stage of air-mist cooling, the wall temperature rapidly decreases due to the effect of latent heat.

REFERENCES

[1] Toda, S. A study of mist cooling (1st report, investigation of mist cooling). *Kikaigakkai Ronbunsshu* (in Japanese) (1972) **38**:581-588.

[2] Rybicki, J.R. and Mudawar, I. Single-phase and two-phase cooling characteristics of upward-facing and downward-facing sprays. *Int. J. Heat Mass Transfer* (2006) **49**:5-16.

[3] Yang, J., Chow, L. and Pais, M. Nucleate boiling heat transfer in spray. *ASME J. Heat Transfer* (1996) **118**:668-671.

[4] Chen, R.H., Chow, L.C. and Navedo, J.E. Effects of spray characteristics on critical heat flux in subcooled water spray cooling. *Int. J. Heat Mass Transfer* (2002) **45**:4033-4043.

[5] Sodtke, C. and Stephan, P. Spray cooling on micro structured surfaces. *Int. J. Heat Mass Transfer* (2007) **50**:4089-4097.

[6] Yoon, G., Yamada, H., Okumiya, M. and Tsujimoto, M. Validation of cooling effectiveness and CFD simulation (study on cooling system by using dry mist). *J. Environ. Eng., AIJ* (in Japanese) (2008) **73**:1313-1320.

[7] Bar-Cohen, A. State-of-the art and trends in the thermal packaging of electronic equipment. *Trans. ASME J. Electronic Packaging* (1992) **114**:257-270.

[8] Waters, R.G., Diode laser degradation mechanisms: A review. *Prog. Quant. Electr.* (1991) **15**:153-174.

[9] Crowe, C.T., Sharma, M.P. and Stock, D.E. The particle-source-in cell (PSI-CELL) model for gas-droplet flows. *Trans. ASME J. Fluids Eng.* (1977) **99**:325-332.

[10] Durbin P.A. Application of a near-wall turbulence model to boundary layers and heat transfer. *Int. J. Heat and Fluid Flow* (1993) 14:316–323.

[11] Launder, B.E. and Spalding, D.B. The numerical computation of turbulent flows. *Computer Methods in Applied Mechanics and Engineering* (1974) **3**:269-289.

[12] Jayatilleke, C.V.L. The influence of prandtl number and surface roughness on the resistance of the laminar sub-layer to momentum and heat transfer. *Progress in Heat and Mass Transfer* (1969) **1**:193-329.

[13] Wang, Y., Li, Y., Weng, S. and Wang, Y. Numerical simulation of counter-flow spray saturator for humid air turbine cycle. *Energy* (2007) **32**:852-860.

[14] Patankar, S.V. *Numerical heat transfer and fluid flow*, New York: Hemisphere, (1980).

[15] Patankar, S.V. and Spalding, D.B. A calculation procedure for heat, mass and momentum transfer in three-dimensional parabolic flows. *Int. J. Heat and Mass Transfer* (1972) **15**:1787-1806.

[16] Van Der Vorst, H.A. Bi-CGSTAB A fast and smoothly converging variant of Bi-CG for the solution of nonsymmetric linear. *SIAM J. Sci. Stat. Comput.* (1992) **13**:631-644.